


Intermittency of three-dimensional perturbations in a point-vortex modelAdrian van Kan,^{*} Alexandros Alexakis[†], and Marc-Etienne Brachet[‡]*Laboratoire de Physique de l'Ecole normale supérieure, ENS, Université PSL, CNRS, Sorbonne Université, Université de Paris, F-75005 Paris, France* (Received 23 December 2020; revised 14 March 2021; accepted 28 April 2021; published 11 May 2021)

Three-dimensional (3D) instabilities on a (potentially turbulent) two-dimensional (2D) flow are still incompletely understood, despite recent progress. Here, based on known physical properties of such 3D instabilities, we propose a simple, energy-conserving model describing this situation. It consists of a regularized 2D point-vortex flow coupled to localized 3D perturbations (“*ergophages*”), such that *ergophages* can gain energy by altering vortex-vortex distances through an induced divergent velocity field, thus decreasing point-vortex energy. We investigate the model in three distinct stages of evolution: (i) The *linear regime*, where the amplitude of the *ergophages* grows or decays exponentially on average, with an instantaneous growth rate that fluctuates randomly in time. The instantaneous growth rate has a small auto-correlation time, and a probability distribution featuring a power-law tail with exponent between -2 and $-5/3$ (up to a cutoff) depending on the point-vortex base flow. Consequently, the logarithm of the *ergophage* amplitude performs a Lévy flight. (ii) The *passive-nonlinear regime* of the model, where the 2D flow evolves independently of the *ergophage* amplitudes, which saturate by non-linear self-interactions without affecting the 2D flow. In this regime the system exhibits a new type of on-off intermittency that we name *Lévy on-off intermittency*, which we define and study in a companion paper [van Kan *et al.*, *Phys. Rev. E* **103**, 052115 (2021)]. We compute the bifurcation diagram for the mean and variance of the perturbation amplitude, as well as the probability density of the perturbation amplitude. (iii) Finally, we characterize the *fully nonlinear regime*, where *ergophages* feed back on the 2D flow, and study how the vortex temperature is altered by the interaction with *ergophages*. It is shown that when the amplitude of the *ergophages* is sufficiently large, the condensate is disrupted and the 2D flow saturates to a zero-temperature state. Given the limitations of existing theories, our model provides a new perspective on 3D instabilities growing on 2D flows, which will be useful in analyzing and understanding the much more complex results of DNS and potentially guide further theoretical developments.

DOI: [10.1103/PhysRevE.103.053102](https://doi.org/10.1103/PhysRevE.103.053102)**I. INTRODUCTION**

Point-vortex flow is a simple (but singular, i.e., weak) solution of the two-dimensional (2D) Euler equation describing inviscid fluid flow, in which N strongly localized vortices advect each other chaotically by their induced velocity fields [1–5]. They admit a famous equilibrium statistical mechanics description due to Onsager [6,7], who showed that states with negative temperatures exist in the system, where same-signed point vortices cluster to form two strong counter-rotating vortices. Indeed, 2D turbulent flow features isolated vortices which aggregate and merge over time in a process called *inverse energy cascade*, forming a large-scale *condensate*, where most of the energy is concentrated in the largest-scale mode [8–10]. This is in contrast with three-dimensional (3D) turbulence, where energy is transferred from large to small scales [11]. Inverse cascades and associated condensation phenomena are also found in quasi-2D flows, such as turbulence in thin layers [12–16] and rapidly rotating turbulence [17,18], which feature 3D components, but are predominantly 2D. A review of such flows is given in Ref. [19].

Point-vortex models have found numerous applications in simplified descriptions of turbulent fluid flows. An early successful simulation of the inverse cascade in 2D turbulence indeed relied on the point-vortex-based vortex-in-cell approximation [20]. In the 1990s, there was a significant activity devoted to vortex gas modeling of (particularly decaying) 2D turbulence [21–25], where merging rules for point vortices were prescribed, yielding 2D turbulence-like behavior at reduced numerical cost. Point-vortex models have also been used to investigate stirring by chaotic advection [26], as well as Lagrangian intermittency, pair dispersion and transport in turbulence [27–29]. Recently, vortex gas scaling arguments were leveraged to find a highly accurate local closure in baroclinic turbulence [30]. Other physical problems which have been fruitfully treated by point-vortex models include the stability of vortex streets and vortex sheets [31–34], quantum turbulence [35–38], plasma dynamics [39] and stellar dynamics [40].

For flows in thin layers, rotating flows and flows under the action of an external magnetic field, it has been proven using upper bound theory [41,42] that a nondimensional threshold exists in terms of the layer depth and fluid viscosity (as well as the rotation rate and or the external magnetic field, if present), where the flow undergoes exact bidimensionalization (for periodic or stress-free boundary conditions). Beyond this point,

^{*} avankan@ens.fr[†] alexakis@phys.ens.fr[‡] marc.brachet@gmail.com

3D perturbations away from a 2D flow decay due to the action of viscous damping. This has profound consequences for turbulent flows since, as mentioned, the phenomenology of 2D turbulence differs strongly from the 3D case due to additional conserved quantities in the 2D case [10,11]. Therefore, it is important to understand quasi-2D flows close to the onset of three-dimensionality. The bounding theory only establishes the existence of a threshold, but since it is built on rather conservative estimates, it cannot capture the physics occurring near the threshold. Very recently, in an extensive numerical study [43], Seshasayanan and Gallet investigated the linear stability of 3D perturbations on a 2D turbulent condensate background flow at the onset of three-dimensionality. The authors showed that when instability is present, the time evolution of the energy of linear 3D modes involves phases of jumplike exponential growth occurring randomly in time, inter-spaced by plateaulike phases where growth is absent. Here, in the spirit of the wide range of applications of point vortices described above, we formulate and analyze a point-vortex model of localized 3D perturbations in quasi-2D turbulence, whose dynamics are qualitatively similar to the exponential growth and decay evolution found in Ref. [43].

The remainder of this article is structured as follows. In Sec. II, we provide a brief introduction to the concept of point-vortex temperature, in Sec. III, we formulate the model to be studied. In Sec. IV, we describe the method of our investigation. Then, in Sec. V we present the results of our numerical simulations and finally in Sec. VI we discuss the implications of our results and remaining open questions.

II. BACKGROUND: TEMPERATURE OF POINT-VORTEX STATES

We briefly summarize the concept of the temperature of point-vortex flow, which was introduced in 1949 by Onsager [6]. The energy of a set of point vortices is given by the Hamiltonian H , which only depends on the vortex positions (x, y) . These positions are the conjugate variables of the point-vortex Hamiltonian. In bounded domains, the total phase space volume is therefore finite. We denote by $\Omega(E)$ the phase space volume occupied by states whose energies H lie in the interval $[E, E + dE]$. Then the thermodynamic entropy is $k_B \ln(\Omega(E)/\Omega_0)$, where k_B is the Boltzmann constant and Ω_0 is a reference volume required for dimensional reasons. In the extreme situation where vortex dipoles (vortex-antivortex pairs) collapse, which corresponds to negative energies $E < 0$, the available phase space volume is vanishingly small, $\Omega(E) \xrightarrow{E \rightarrow -\infty} 0$. The opposite limit of large positive energies occurs when like-sign vortices concentrate at a point, in which case also $\Omega(E) \xrightarrow{E \rightarrow \infty} 0$. Since the total volume is nonzero, the nonnegative function $\Omega(E)$ must reach a maximum at an intermediate energy $-\infty < E_m < \infty$. The associated microcanonical inverse temperature,

$$\beta(E) \equiv \frac{\partial \ln[\Omega(E)]}{\partial E}, \quad (1)$$

is thus positive for $E < E_m$, but vanishes at $E = E_m$ and is negative for $E > E_m$. Negative-temperature states can generally arise in both classical and quantum systems with a finite

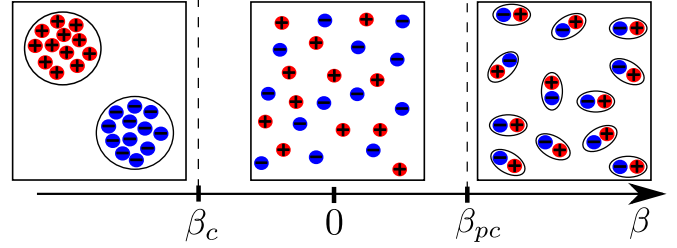


FIG. 1. Overview of point-vortex states at negative, zero and positive inverse temperatures β . Clustering occurs for $\beta < \beta_c < 0$, a homogeneous state is found at $\beta = 0$, and pair condensation occurs for $\beta > \beta_{pc}$.

number of degrees of freedom whose state space is bounded, such as localized spin systems [44–46]. In the point-vortex system, high-energy states at negative temperatures, corresponding to condensates featuring same-sign vortex clusters, have been extensively studied since Onsager’s initial contribution [6,7,47,48]. In particular, there is a negative clustering temperature β_c , which marks the onset of same-sign vortex clustering. Similarly, there is a positive pair condensation temperature β_{pc} , at which opposite-sign vortices form dipole pairs which propagate through the domain, see Ref. [49]. The vanishing inverse temperature at $E = E_m$ corresponds to a homogeneous state with positive and negative vortices spread out evenly over the domain. The point-vortex states at different temperatures are summarized in Fig. 1. Such point-vortex states at any given inverse temperature β may be generated using the noisy gradient method presented in Appendix B, which was previously introduced in Ref. [50]. Specifically, once a statistically stationary state is reached, this numerical method generates random point-vortex states according to the canonical distribution associated with the inverse temperature β . For a given value of β , the mean energy in the statistically stationary state can be measured from the time series. Thus, like every microcanonical temperature corresponds to an energy E according to Eq. (1), in the noisy gradient method every value of β corresponds to a mean energy $\langle E \rangle$ in steady state. The resulting mean energy as a function of temperature is shown in Fig. 2.

III. THE MODEL

Here we construct the simplified model of the interaction of 2D and 3D flow studied in this paper. The model is in the same spirit as shell models of turbulent cascade processes [51], which replace the Navier-Stokes dynamics with a simpler set of coupled nonlinear ordinary differential equations, which conserve a number of quantities including total energy and enstrophy in the 2D case, aiming at providing insights into turbulent cascade processes. The present model, as we show below, may similarly provide insights into the dynamics of 3D instabilities on turbulent 2D flows.

For the sake of simplicity and clarity, the theoretical formalism is presented in the infinite domain. In Appendix A, we provide the equations for the 2D doubly periodic domain $[0, 2\pi L] \times [0, 2\pi L]$, where the statistical point-vortex temperature from Sec. II is well defined.

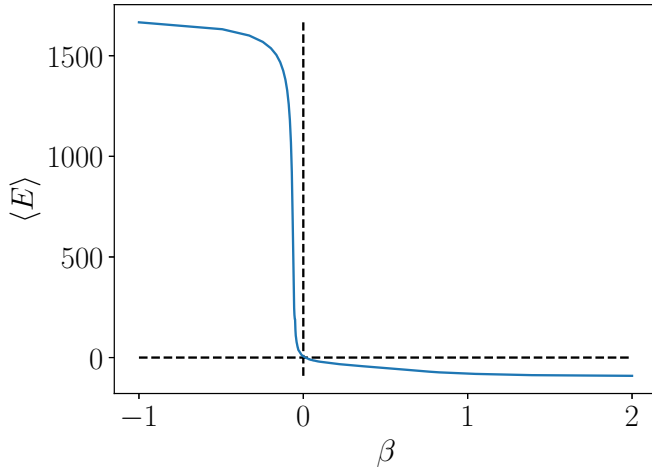


FIG. 2. Mean point-vortex energy $\langle E \rangle$ of $N_v = 32$ vortices versus β , computed using the method described in Appendix B in the periodic domain $[0, 2\pi] \times [0, 2\pi]$ (with a truncation at distances smaller than $\epsilon = 0.1$, cf. Appendix B). This curve allows a translation from vortex energies at steady state to corresponding temperatures.

Our main goal is to arrive at a model of minimum complexity describing the growth of 3D perturbations on a 2D large-scale condensate flow. Two key ingredients must be selected. First, a model of the two-dimensional base flow must be chosen. Here we opt for 2D point-vortex flow, in view of its many successful modeling applications to two-dimensional turbulent flows, as presented in the introduction. Specifically, we consider an even number N_v of point vortices with circulations $\Gamma_i = \Gamma$ for odd i and $\Gamma_i = -\Gamma$ for even i , located at positions $\mathbf{x}_v^{(i)} = (x_v^{(i)}, y_v^{(i)})$.

Second, the 3D perturbations have to be modelled. While there exist 3D vortex filament models, commonly used in quantum turbulence, which describe mutual advection of curved vortex lines [52,53], these are significantly more complex than their 2D counterparts—in particular, each segment of every vortex line is advected by all other vortex lines via the Biot-Savart law, and in addition proper handling of vortex reconnections is a complicating factor. Instead, here we seek a simpler description. Simulations of turbulent flows close to the onset of three-dimensionality reveal that 3D perturbations are strongly localized (spatially intermittent) in the 2D plane [14,15,43]. Indeed, close to the onset of three-dimensionality, high wavenumbers in the third dimension are suppressed by viscous damping. Hence, the 3D instability, while being strongly localized in the 2D plane, is also expected to have a simple spatial structure in the third dimension, and its intensity can be approximately characterized by a single scalar amplitude.

Combining these two insights, we model 3D motions as N_p localized, pointlike entities in the plane whose detailed spatial structure in the third dimension is ignored, and whose intensity is characterized by an effective perturbation amplitude A_k , for $k = 1, \dots, N_p$. We name these entities “ergophages” and denote their positions by $\mathbf{x}_p^{(k)} = (x_p^{(k)}, y_p^{(k)})$. While the model describes 3D flow, the mathematical structure of the model is effectively 2D. We stress that this is not a contradiction,

since the reduction is based on the physical properties of 3D perturbations close to onset, and retains 3D information.

Point vortices and 3D perturbations induce velocity fields that advect each other following the equations:

$$\frac{d}{dt} \mathbf{x}_v^{(i)} = \mathbf{U}_v^{(i)} + \mathbf{U}_p^{(i)} + \mathbf{u}_f^{(i)} \quad (2)$$

and

$$\frac{d}{dt} \mathbf{x}_p^{(k)} = \mathbf{U}_v^{(k)} + \mathbf{v}_f^{(k)}, \quad (3)$$

where $\mathbf{U}_v^{(i)}$ is the velocity induced on vortex i by all point vortices $i \neq j$, $\mathbf{U}_p^{(i)}$ is the velocity induced on vortex i by the 3D ergophages and $\mathbf{U}_v^{(k)}$ is the velocity induced on ergophage k by all N_v point vortices. Finally, $\mathbf{u}_f^{(i)}$ and $\mathbf{v}_f^{(k)}$ are externally imposed velocity fields that could inject energy to the system. Also, note that ergophages do not advect each other, a choice which is made for simplicity—mutual advection of ergophages can easily be included in the model presented below (while this was not studied in detail, it did not seem to affect the qualitative model behavior).

In the absence of ergophages and external velocities, the model reduces to classical point-vortex flow. In this case, point vortices move due to their mutual advection, following Hamiltonian dynamics so that the velocity field $\mathbf{U}_v^{(i)}$ can be written as

$$\mathbf{U}_v^{(i)} = \Gamma_i^{-1} \begin{pmatrix} \partial_{y_v^{(i)}} H \\ -\partial_{x_v^{(i)}} H \end{pmatrix}, \quad (4)$$

corresponding to the advection of the i th vortex by all vortices $j \neq i$. The Hamiltonian H in \mathbb{R}^2 is given by

$$H(x_v^{(1)}, \dots, x_v^{(N_v)}) = -\frac{1}{2} \sum_{\substack{i,j=1 \\ i \neq j}}^{N_v} \Gamma_i \Gamma_j \log(|\mathbf{x}_v^{(i)} - \mathbf{x}_v^{(j)}|), \quad (5)$$

which is a sum over pairs depending on the vortex-vortex distances alone. The velocity field $\mathbf{U}_v^{(k)}$ closely resembles $\mathbf{U}_v^{(i)}$, but it includes the advection due to all N_v vortices, formally omitting the condition $i \neq j$ in H before differentiating in Eq. (4) and evaluating at $\mathbf{x}_v^{(i)} \rightarrow \mathbf{x}_p^{(k)}$. The Hamiltonian also gives the kinetic energy of the flow (up to a factor of $(2\pi)^{-1}$ times the constant fluid density, and an additive infinite constant due to self-energy), which is conserved. The point-vortex energy increases when same-sign vortices approach each other and when opposite-sign vortices move apart, while it decreases when same-sign vortices move apart and when opposite-sign vortices approach each other.

In the presence of ergophages, energy of the 2D field can be transferred to the 3D field perturbations. Thus, to gain energy, an ergophage must reduce the energy of a given point-vortex configuration on which it is superimposed. Each ergophage induces a 3D perturbation velocity field $\mathbf{u}_p^k(\mathbf{x})$ of amplitude A_k^2 . Importantly, despite the model being formally 2D, the fact that ergophages represent 3D structures implies that $\mathbf{u}_p^k(\mathbf{x})$ has a nonzero divergence in the (x, y) plane. This is in contrast to the velocity field $\mathbf{U}_v^{(i)}(\mathbf{x})$ induced by 2D point vortices, whose 2D divergence vanishes. The total velocity field induced by

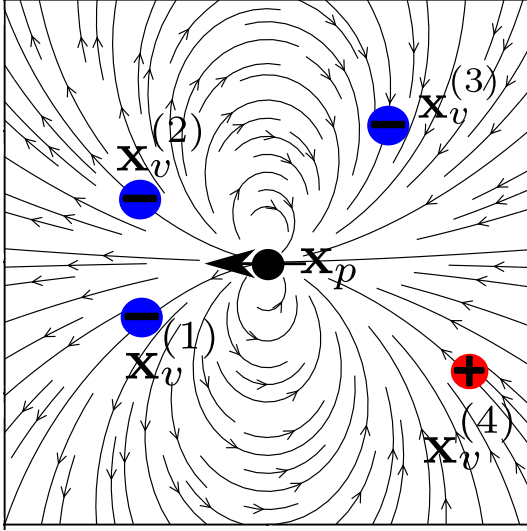


FIG. 3. Illustration of how a velocity field \mathbf{u}_p (stream lines) due to a 3D perturbation at \mathbf{x}_p , can reduce point-vortex energy. This is done by increasing the distance between the same-sign vortices at $\mathbf{x}_v^{(1)}$, $\mathbf{x}_v^{(2)}$ and/or decreasing the distance between opposite-sign vortices at $\mathbf{x}_v^{(3)}$, $\mathbf{x}_v^{(4)}$. The bold black arrow passing through \mathbf{x}_p represents the dipole moment.

the ergophages is then given by

$$\mathbf{U}_p(\mathbf{x}) = \sum_{k=1}^{N_p} A_k^2 \mathbf{u}_p^{(k)}(\mathbf{x}), \quad (6)$$

such that the velocity induced on vortex i can be written as $\mathbf{U}_p^{(i)} = \mathbf{U}_p(\mathbf{x}_v^{(i)})$. This field modifies the point-vortex positions and thus their energy, allowing ergophages to grow under suitable conditions.

Our choice for $\mathbf{u}_p^{(k)}(\mathbf{x})$ should be the simplest possible. It is shown in the Appendix D that the choice of a monopole, which at first does suggest itself for its simplicity, cannot produce 3D instability. Hence, the simplest nontrivial choice for $\mathbf{u}_p^{(k)}(\mathbf{x})$ is given by a dipole field,

$$\mathbf{u}_p^{(k)} = (\hat{d}_k \cdot \nabla) \left(\frac{\partial_x \phi^{(k)}}{\partial_y \phi^{(k)}} \right), \quad (7)$$

where $\hat{d}_k = [\cos(\varphi_k), \sin(\varphi_k)]$ is the dipole moment with φ_k the angle between the dipole moment and the x -axis. The potential $\phi^{(k)}$ is given by

$$\phi^{(k)}(\mathbf{x}) = -\frac{1}{2}c \log(|\mathbf{x}_p^{(k)} - \mathbf{x}|), \quad (8)$$

where c is a coupling coefficient. An example of dipole interactions is shown in Fig. 3. In this case the perturbation velocity field makes same-sign vortices approach each other (e.g., $\mathbf{x}_v^{(1)}$ and $\mathbf{x}_v^{(2)}$ in Fig. 3) and opposite-sign vortices move apart (e.g., $\mathbf{x}_v^{(3)}$ and $\mathbf{x}_v^{(4)}$ in Fig. 3), thus reducing the point-vortex energy. Now, assume one were to interchange $\mathbf{x}_v^{(1)} \leftrightarrow \mathbf{x}_v^{(4)}$ and $\mathbf{x}_v^{(2)} \leftrightarrow \mathbf{x}_v^{(3)}$ in Fig. 3, keeping \mathbf{x}_p the same. The dipole field would then cause an increase in point-vortex energy and thus would no longer lead to any 3D instabilities. However, it suffices to rotate the dipole moment by 180° to recuperate a 3D instability. This example illustrates that the dipole field can

lead to 3D instability for a given vortex configuration (even if monopole field would not), provided that the orientation of the dipole moment is suitably chosen. For simplicity the dipole moment in this work will always be chosen such as to ensure maximum (positive) energy extraction from the 2D field.

In our model we assign to the ergophages the 3D energy

$$E_{3D} = \frac{1}{2} \sum_k A_k^2. \quad (9)$$

The energy exchanges between 2D and 3D flow must be conservative. Thus, any decrease of the point-vortex energy should correspond to an increase of 3D ergophage energy. We let the amplitudes A_k evolve according to

$$\frac{dA_k}{dt} = (\gamma_k - \nu)A_k - \delta A_k^3 \quad (10)$$

(no implicit summation), where γ_k is an instantaneous growth rate due to interactions with the point vortices, ν (proportional to viscosity) is a linear damping coefficient and δ is a nonlinear damping coefficient due to self-interactions. Such nonlinear effects in three-dimensional velocity fields are associated with a Kolmogorov forward energy cascade, whose amplitude will generally depend on system parameters, such as domain geometry and system rotation rate. Hence the coefficient δ should also depend on these system parameters. In order for the coupling to conserve energy, the growth-rate is given by

$$\gamma_k = - \sum_{i=1}^{N_v} \mathbf{u}_p^{(k)}(\mathbf{x}_v^{(i)}) \cdot \nabla_{\mathbf{x}_v^{(i)}} H. \quad (11)$$

As is shown in Appendix C, these model equations imply that the total energy

$$E_{\text{tot}} = H + \frac{1}{2} \sum_{k=1}^{N_p} A_k^2 = H + E_{3D} \quad (12)$$

is conserved, provided $\mu = \delta = 0$ (no dissipation) and $\mathbf{u}_f = \mathbf{0}$ (no energy injection). Note that for E_{tot} to be dimensionally consistent, A_k must have dimensions of circulation. In addition to the energy, the 2D Euler equation conserves the so-called Casimir invariants, which are of the form $\int \omega^n d^2x$, ($n = 2$ gives the enstrophy), where ω denotes vorticity. In the point-vortex model, the vorticity depends only on the number and circulation of vortices, both of which are conserved in our model.

In the presence of dissipation it is useful to have a driving mechanism as well, so that a nontrivial steady state is reached. This is achieved by the choice

$$\mathbf{u}_f^{(i)} = \epsilon_f [\nabla_{\mathbf{x}_i} H + |\beta_f|^{-1/2} \boldsymbol{\eta}_i(t)], \quad (13)$$

where $\boldsymbol{\eta}_k(t) = (\eta_k^1(t), \eta_k^2(t))^T$ with independent white Gaussian noise components η_k^i satisfying $\langle \eta_k^i(t) \rangle = 0$ and $\langle \eta_k^i \eta_{k'}^j \rangle = 2\delta_{i,i'} \delta_{k,k'} \delta(t - t')$ for the ensemble average $\langle \cdot \rangle$. In the absence of ergophages, this noisy-gradient driving leads to a point-vortex flow with temperature β_f^{-1} and is described in detail in Appendix B. We emphasize that the driving Eq. (13) can either increase or decrease the 2D energy. If the 2D energy at any given time is above the equilibrium value corresponding to the temperature β_f^{-1} (shown in Fig. 2), then the driving will

act to decrease energy to the equilibrium value. Conversely, if the 2D energy is below that equilibrium value, the driving will act to increase the 2D energy. We also point out that, as a consequence of the inverse energy cascade, 2D flows typically feature the formation of large-scale coherent structures at late times. Such a structure is observed in the point-vortex system at negative β . At intermediate stages of the inverse cascade process, for instance if the cascade is interrupted by large-scale friction, one finds an approximately homogeneous gas of vortices [54]. In the point-vortex system, this is realized when $\beta \approx 0$. At $\beta > 0$, the point-vortex model is characterized by vortex-antivortex bound states. To the best of our knowledge, however, these are never observed in laboratory experiments [13,55] nor numerical studies [12,14,15] of turbulent quasi-2D flows. We conclude that the regime $\beta \leq 0$ is the physically relevant one.

Finally, since the total energy is independent of the ergophage positions, we chose \mathbf{v}_f to be a noise term, without altering the energy dynamics,

$$\mathbf{v}_f^{(k)} = \sigma \boldsymbol{\eta}_k(t), \quad (14)$$

where $\eta_i = (\eta_i^{(1)}, \eta_i^{(2)})$, with $\eta_i^{(j)}$ pairwise independent zero-mean white Gaussian noise terms. The noise is added to eliminate a remaining dependence on initial conditions. Note that in our model, different ergophages do not directly affect each other, neither in terms of their amplitudes, nor their positions. They can only affect each other indirectly by altering the background 2D flow nonnegligibly and thus changing the growth rate γ_k experienced by each ergophage. This is mainly motivated by our goal of maximum simplicity. First, the model 3D energy is independent of ergophage positions, thus we may decide to neglect mutual advection of ergophages in a minimal description of how 3D energy evolves. Second, while in a strongly 3D flow, the 3D components of the flow will feed back on one another, the growth or decay of 3D perturbations at small to moderate 3D amplitudes on a primarily 2D flow should be mainly determined by direct interactions between 2D and 3D components, rather than interactions between 3D and 3D components.

Equations (2), (3), and (10) define the time evolution of our model, which we solve numerically in the following sections.

IV. NUMERICAL IMPLEMENTATION

We developed a fully MPI-parallelized Fortran program, using a fourth-order Runge-Kutta time stepper, to simulate the model in the 2D doubly periodic domain $[0, 2\pi L] \times [0, 2\pi L]$, based on the Weiss-McWilliams formalism introduced in Ref. [56]. The parallelization is implemented by assigning a subset of vortex-vortex pairs and vortex-ergophage pairs to each processor, over which to sum when computing quantities involving such pairs such as $\mathbf{U}_v^{(i)}$, $\mathbf{U}_p^{(i)}$, H , and γ_k . The specific model equations for the periodic domain are given in Appendix A. Since the periodic domain has a finite area, the statistical point-vortex temperature introduced in Sec. II is well defined here and no vortices can escape to infinity. A regularization was introduced at distances smaller than a positive cutoff $\epsilon \ll 2\pi L$ (we set $\epsilon/(2\pi L) = 0.015$), similarly as in Ref. [34]. This regularization is required to avoid blow-ups,

i.e., events where the time step required by the CFL condition [57] for well-resolvedness becomes extremely small. The way the cutoff is introduced approximately corresponds to smearing out the delta-peaked vorticity over a circular patch of constant vorticity, also known as a *Rankine vortex* [58]. In a realistic turbulent flow, there is a cutoff at small length scales related to viscosity. We note that vortex merging does not occur in the point-vortex model used here, with or without a cutoff (however, it may be added explicitly as in Refs. [21–25]). The time step Δt for the Runge-Kutta scheme is dictated by the maximum growth rate γ_k , which is associated with close encounters where some distances are of the order of ϵ . For highly condensed configurations, where $N_v/2$ vortices form a cluster for each sign of circulation, each cluster comprises approximately $N_v^2/8$ vortex pairs contributing to γ_k . At small distances $|\mathbf{u}_p^{(k)}| = O(\epsilon^{-2})$ and $|\nabla_{\mathbf{x}_v^{(i)}} H| = O(\epsilon^{-1})$, such that the time step thus bounded above by

$$\Delta t \lesssim [\max(\gamma_k)]^{-1} \propto \frac{8\epsilon^3}{N_v^2}. \quad (15)$$

For dilute vortex configurations, the largest growth rates stem from encounters between a single ergophage and a single vortex, such that $\Delta t \lesssim \epsilon^3$. This strong dependence of the required time step on the cutoff ϵ , and the number of vortices N_v for dense configurations, is an important limiting factor in terms of computational cost. The operation of the highest numerical complexity at every time step is the evaluation of γ_k , since it requires summing $O(N_v^2)$ vortex-vortex pairs for every $k = 1, \dots, N_p$.

V. SIMULATION RESULTS

To study the model introduced in Sec. III, we first use the noisy gradient method described in Appendix B to generate point-vortex states with $N_v = 32$ vortices at both positive and negative temperatures. This relatively small number of vortices is chosen to be able to run simulations for long times to obtain satisfactory statistics. The energy of the resulting equilibria as a function of their inverse temperature β is as shown in Fig. 2. We note that at this relatively low number of vortices, the transitions to a condensate and to pair condensation are not sharp. Using these states generated by the noisy gradient method as initial conditions for the point vortices, we proceed in the three following steps:

(A) The passive, linear regime: perturbation amplitudes $A_k/\Gamma \ll 1$ and $\delta \rightarrow 0$ for a given background point-vortex flow. In this limit, the evolution Eq. (10) of A_k is linear and the point-vortex energy H is constant in time since $\mathbf{U}_p = O(A_k^2)$ is negligible with respect to the conservative Hamiltonian advection terms. To investigate this limit we set $\mathbf{U}_p = 0$ in Eq. (3) and $\delta = 0$ in Eq. (10). Since there is no dissipation in the system we also set $\mathbf{u}_f = 0$.

(B) The passive, nonlinear regime: still $A_k/\Gamma \ll 1$, such that H still remains unaffected by the 3D instabilities, but we include saturation of the amplitude A_k due finite δ , i.e., nonlinear self-interaction (in both the linear and passive nonlinear regimes, individual 3D perturbations evolve independently). In this limit $\mathbf{U}_p = \mathbf{u}_f = 0$ in Eq. (3) as well.

(C) The fully nonlinear regime, where the amplitudes $A_k/\Gamma = O(1)$, thus the induced ergophage velocity \mathbf{U}_p is fi-

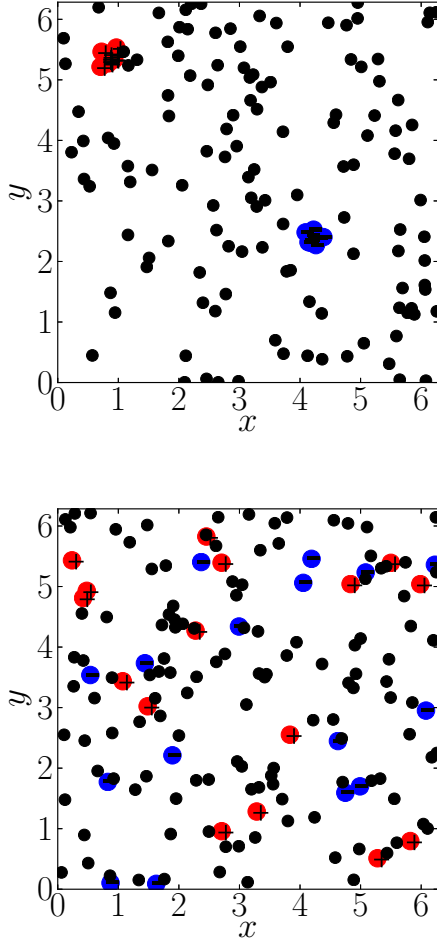


FIG. 4. Snapshots from two simulations with $N_p = 128$ perturbations (black dots) evolving on a point-vortex flow consisting of $N_v = 32$ individual vortices, which is highly condensed at $\beta = -\frac{1}{8}$ (top) and dilute at $\beta = -\frac{1}{128}$ (bottom).

nite and its effect on point vortices cannot be neglected. In this case H is no longer conserved. To sustain the dynamics against dissipation, the “driving” term \mathbf{u}_f given in Eq. (13) is included.

A. The passive linear regime

We initialize the simulation with $N_v = 32$ vortices at an inverse temperature $\beta < 0$, with half of the vortices having circulation $\Gamma_i = \Gamma$, and the other half having circulation $\Gamma_i = -\Gamma$. In addition, we introduce $N_p = 128$ randomly placed ergophages of some small initial amplitude (the same for every perturbation). It is worth reiterating that in the linear phase of the evolution, since there is no feedback on the flow, each ergophage is evolving independently from all the others. Furthermore in the linear phase the effect of the damping parameter ν is to induce a mean exponential decay. The time evolution of $A_k(t, \nu)$ for any value of ν can thus be recovered from the $\nu = 0$ case as $A_k(t, \nu) = A_k(t, 0)e^{-\nu t}$. For this reason only the $\nu = 0$ case is examined and the growth rate γ'_k of a $\nu \neq 0$ case is obtained as $\gamma'_k = \gamma_k - \nu$.

The configuration under investigation is illustrated in Fig. 4 for a highly condensed case ($\beta = -\frac{1}{8}$) and a dilute case ($\beta =$

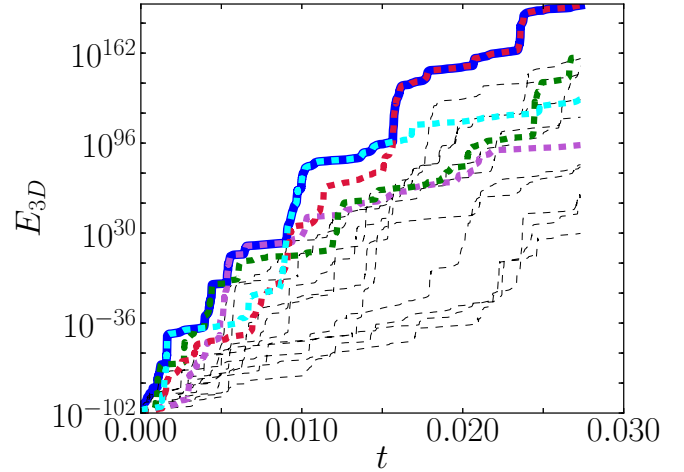


FIG. 5. Lin-log plot showing the time series of the energy of $N_p = 128$ localized 3D perturbations (total energy shown in solid blue, selected individual contributions $\frac{1}{2}A_k^2$ in dashed black lines) in the passive linear regime with $\nu = 0$, growing on a highly condensed background 2D flow at $\beta = -\frac{1}{8}$.

$-\frac{1}{128}$). Then we let the system evolve in time and obtain a time series like the one shown in Fig. 5 for the highly condensed case, where the 3D energy (solid blue line) alternates between plateaulike phases of slow growth and phases of abrupt exponential growth. The time series bears resemblance to that obtained from the complete linear stability analysis of 3D instabilities on a turbulent 2D flow performed by Seshasayanan and Gallet (see Fig. 1 in Ref. [43]). In the same Fig. 5, we also show the energy of individual ergophages, $\frac{1}{2}A_k^2$, by dashed lines. Their sum is equal to the blue solid line.

Two points need to be made. First, one observes in the time evolution of individual ergophages that there are alternating phases of slow growth/stagnation and of rapid exponential growth. Second, at a given time t , $E_{3D}(t)$ is dominated by the ergophage with the largest amplitude $A_k(t)$. Abrupt growth events in E_{3D} also occur when another ergophage $A_{k'}$ grows exponentially and “overtakes” A_k , thereby leading to abrupt growth of the sum.

Each of the N_p localized perturbations experiences a different, time-varying growth rate $\gamma_k(t)$. To understand this linear growth, we need to quantify the statistical properties of these random growth rates.

In Fig. 6, we plot histograms of γ_k sampled over all $k = 1, \dots, N_p$ and all time steps. In both cases, one observes a power-law range in the PDF. For the dilute case ($\beta = -\frac{1}{128}$) the power-law exponent is close to -2 , while for the dense state ($\beta = -\frac{1}{8}$) it is closer to $-5/3$. These two exponents can be understood if one identifies the dominant interactions.

In the dilute case $|\beta| \ll 1$, where point vortices are far apart, an ergophage maximizes its energy extraction when being close to a single point vortex. It does so by displacing the vortex towards the nearest opposite-sign vortex and/or further apart from the nearest same-sign vortex.

In the dense (condensate) case $-\beta \gg 1$, point vortices form high-density, same-signed clusters. In order for an ergophage to maximize energy extraction, it needs to be located close to these clusters.

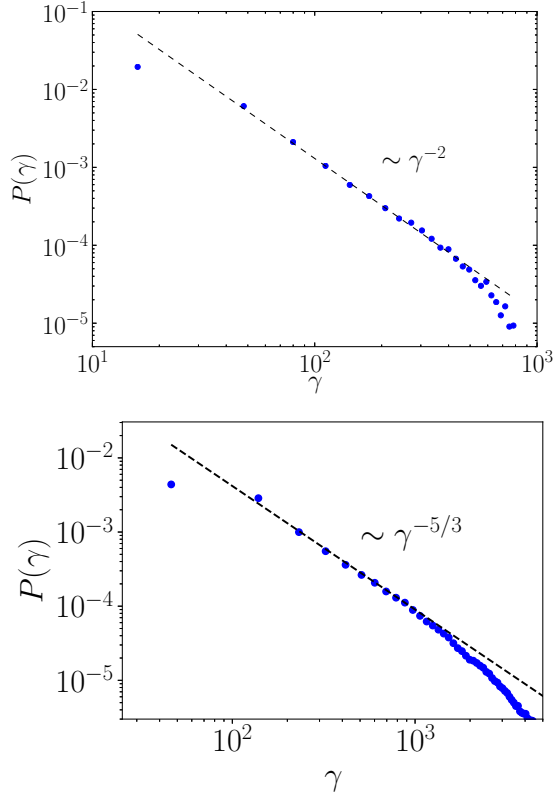


FIG. 6. Two histograms of the growth rate γ_k , sampled over all time steps and all 128 ergophages from the run corresponding to the two linear simulations with a dilute vortex state at $\beta = -1/128$ (top) and a condensed vortex state at $\beta = -1/8$ (bottom) visualized in Fig. 4. Power-law ranges with exponents -2 and $-5/3$ can be discerned, as predicted for dilute and dense vortex base states, respectively.

The PDF of the growth rate γ_k can then be calculated by assuming that all positions in space are equally probable and that at each time it is the interaction with the closest pair of point vortices that dominates. A detailed calculation, given in Appendix E, yields

$$P(\gamma) \propto \gamma^{-2} \quad \text{at large } \gamma, \quad (16)$$

for the dilute limit $|\beta| \ll 1$, while for the dense limit $-\beta \gg 1$ one obtains

$$P(\gamma) \propto \gamma^{-5/3} \quad \text{at large } \gamma. \quad (17)$$

The predicted power laws agree with the PDFs obtained numerically. Note, however, that in our numerical set-up these results are valid up to a large- γ cutoff resulting from the regularization at distances less than ϵ . This is important because without this regularization, the variance and the mean would be infinite for the power-law PDFs of γ_k found here. This implies that some of the results observed here have an explicit dependence on ϵ .

Besides the growth-rate distribution, to characterize the statistical properties of γ_k we also need to quantify its auto-correlation time τ_{ac} .

We define τ_{ac} in terms of the normalized auto-correlation function $\Gamma(\tau) = \langle \gamma(t)\gamma(t+\tau) \rangle / \langle \gamma(t)^2 \rangle$, as the smallest τ

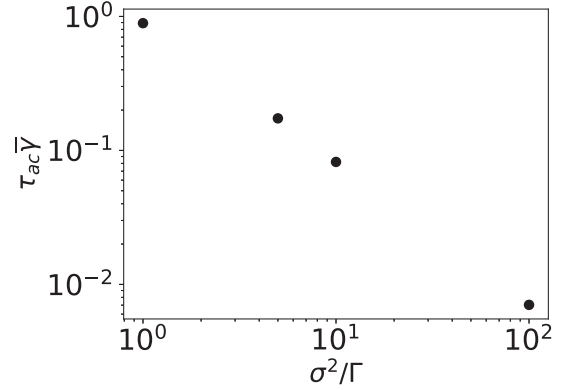


FIG. 7. Log-log plot of the auto-correlation time τ_{ac} of the growth rate γ (see text for the definition of τ_{ac}) in a passive, linear simulation at $\beta = -1/16$, nondimensionalized by the mean growth rate, versus the squared amplitude of the noise acting on 3D perturbations, nondimensionalized by the r.m.s. vortex circulation.

for which $\Gamma(\tau) \leq 0.5$, where $\Gamma(0) = 1$ by definition and $\langle f(\gamma) \rangle = \frac{1}{N_p T} \int_0^T dt \sum_{k=1}^{N_p} f(\gamma_k(t))$ is an average over time t (T is the time at the end of the simulation) and realizations (ergophages). We stress that the small-distance cutoff introduced in the velocity field, leading to a large- γ cutoff in $P(\gamma)$ is essential for obtaining a finite mean growth rate $\langle \gamma \rangle$ and finite variance, since a PDF featuring power-law tails with exponents -2 , $-5/3$ does not have a finite mean or variance otherwise.

Figure 7 shows that the auto-correlation time decreases monotonically with σ [defined in Eq. (14)], as $\tau_{ac} \sim \sigma^{-2}$. By increasing σ sufficiently, one obtains an arbitrarily small auto-correlation time. When $\tau_c \langle \gamma \rangle \ll 1$, the random process $\gamma_k(t)$ can be approximated as uncorrelated in time.

Summarizing the above findings, the increments of A_k are randomly distributed according to a PDF with power law tails whose exponents are between -2 and $-5/3$ and approximately white in time since it is uncorrelated in time beyond a small correlation time (for sufficiently large σ). These properties imply that the evolution of A_k due to γ_k is well approximated by a Lévy flight process.

A Lévy flight is a random process with independent stationary increments η , where the increments follow a heavy-tailed PDF. By the generalized central limit theorem [59], the sum of many such heavy-tailed increments follows a stable PDF $P_{\alpha, \tilde{\beta}}(\eta)$ depending on two parameters $\alpha \in (0, 2]$ and $\tilde{\beta} \in [-1, 1]$. Lévy flights were first introduced in Ref. [60] and have since found numerous applications in physics and beyond [61,62]. The influence of α , $\tilde{\beta}$ on the PDF $P_{\alpha, \tilde{\beta}}(\eta)$ is as follows. For $\alpha = 2$, one obtains the Gaussian distribution. For $\alpha < 2$, a stable distribution features power-law tails $P(\eta) \propto \{1 + \tilde{\beta} \text{sign}(\eta)\} |\eta|^{-\alpha-1}$ at $|\eta| \rightarrow \infty$. The parameter $\tilde{\beta}$ measures the asymmetry of PDF. For $\tilde{\beta} = 1$ and $\alpha < 1$, one obtains a one-sided PDF with support on \mathbb{R}_+ only. Stable PDFs are known to occur for velocity and velocity difference statistics in 2D vortex flows in particular [63]. The fact that the PDF of γ_k shows power-law tails in our model can be understood as a consequence of this property of 2D vortex flows.

If γ_k is interpreted as noise, then Eq. (10) is a stochastic differential equation with multiplicative Lévy noise whose parameters depend on the 2D flow temperature. The dense and dilute cases described above, for which the γ_k PDF has power law ranges with exponents $-5/3$ and -2 , respectively, correspond to noise parameters $\alpha = 2/3$ and $\alpha = 1$, respectively, and $\beta = 1$ since the linear growth rate γ_k is positive definite in the model by construction.

The theory of systems with multiplicative Gaussian white noise has found a plethora of applications, in particular to noise-induced transitions [64] and the phenomenon of on-off intermittency [65–67]. While the role of long-time correlated noise in on-off intermittency has been considered before [68–71], the case of on-off intermittency with heavy-tailed noise has not previously been studied explicitly, to our knowledge. Our companion paper [72] is devoted to this topic. Here we summarize only the relevant results. It is shown in Ref. [72] that in the case $\alpha < 1$ and $\beta = 1$, which applies here, the system Eq. (10), with γ_k interpreted as white Lévy noise, is unstable for all values of ν : since the mean value of $\langle \gamma_k \rangle \rightarrow +\infty$, viscosity ν , no matter how large, cannot stop the growth of A_k . If, however, the possible values γ_k are restricted (“truncated”) to be below some maximum, so that a finite value of $\langle \gamma_k \rangle$ exists, then there is a critical value of viscosity ν_c above which all trajectories converge to zero $A_k \rightarrow 0$. However, this critical value depends on the truncation value of γ_k , which implies that the threshold ν_c will depend on the regularization cutoff ϵ . At long time scales the system displays on-off intermittency.

B. The passive nonlinear regime

We solve the model equations for $N_p = 32$ passive nonlinear dipole ergophages evolving on a highly condensed background flow of $N_v = 32$ point vortices at temperature $\beta = -1/8$, fixing the nonlinear damping coefficient at $\delta = 1$. For a given ν , we initialize the ergophages at random positions and with small amplitudes. We let the system evolve for long times, such that the perturbation amplitude either decays or reaches a statistically steady state. We then measure the steady-state time average of the moments $M_n = \langle A^n \rangle$, in terms of $\langle f(A) \rangle = \lim_{T \rightarrow \infty} \frac{1}{TN_p} \int_0^T \sum_{k=1}^{N_p} f(A_k) dt$. We also define the “zeroth” moment as $M_0 = \exp(\langle \log(A) \rangle)$. By the inequality of arithmetic and geometric means the moments are ordered $M_0 \leq M_1 \leq M_2^{1/2} \leq M_3^{1/3} \leq \dots$. The resulting bifurcation diagram of M_0, M_1, M_2 as a function of ν is shown in Fig. 8.

On-off intermittency predicts that all nonzero moments scale linearly with $\nu_c - \nu$, $M_n \propto (\nu_c - \nu)$, while the zeroth moment scales as $M_0 \propto \exp(-cst./(\nu_c - \nu))$. Comparing this with the bifurcation diagram shown in Fig. 8, where the scalings from the Gaussian case are shown by dashed lines, one sees that the time-averaged moments and the Gaussian scalings agree well within the errorbars. This is a consequence of the truncation in the model, which subjects the statistics to a convergence to the Gaussian case, albeit “ultraslow” [73], by the central limit theorem after the sample averaging and/or long-time averaging procedures.

Another prediction of on-off intermittency is that the PDF of the unstable field shows an integrable powerlaw divergence

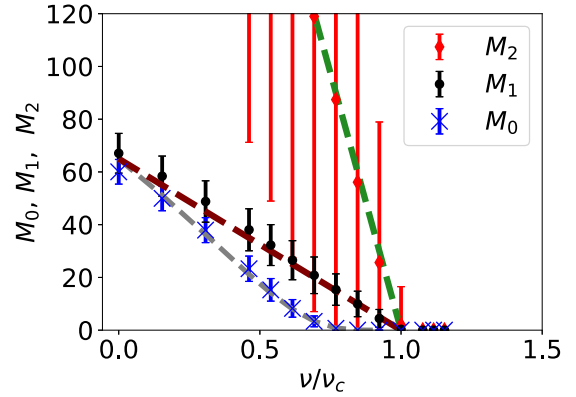


FIG. 8. Bifurcation diagram for $N_p = 32$ passive nonlinear (i.e., independent) dipole ergophages on the background flow at $\beta = -1/8$, $\delta = 1$. The values of $\langle X \rangle_n$ is averaged over the statistically steady state. Error bars are given by the sample standard deviation of the time series in steady state. The dashed lines show the scalings from the Gaussian noise case.

at zero amplitude with an exponent that approaches the value -1 from above as $\nu \rightarrow \nu_c$, while an exponential cutoff is expected for large values of A_k . Figure 9 shows the PDF of A_k . At small values of A the PDF displays a power law A^κ with κ approaching -1 as $\nu \rightarrow \nu_c$ in agreement with the Gaussian on-off prediction. At large A the PDF shows a steeper power-law scaling. In the companion paper [72], the asymptotics $P(A) \propto A^{-3} \log^{-2/3}(A)$ at large values of A are derived analytically from a fractional Fokker-Planck equation associated with Eq. (10) for nontruncated multiplicative Lévy noise with parameters $\alpha = 2/3$, $\beta = 1$ (in the Stratonovich interpretation), which fits the present data well. Since $A^{-1} \log^{-\alpha}(A)$ is only integrable at $A \rightarrow \infty$ for $\alpha > 1$, the scaling $P(A) \propto A^{-3} \log^{-2/3}(A)$ implies that without a cutoff, only the mean is finite, while the variance and all higher moments diverge. With a cutoff at length ϵ , all moments are finite, but only the mean is of order one, while all higher moments depend

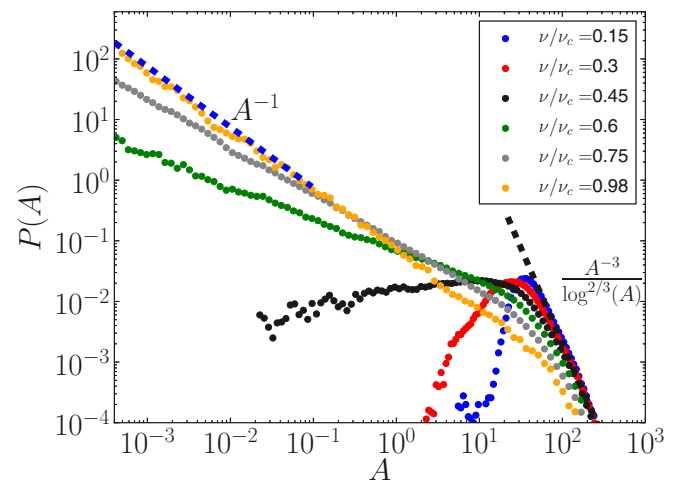


FIG. 9. Steady state PDF of ergophage amplitudes from the numerical solution of the model in the passive nonlinear regime for $\delta = 1$, $\nu/\nu_c = 0.15$ on the background flow at $\beta = -1/8$.

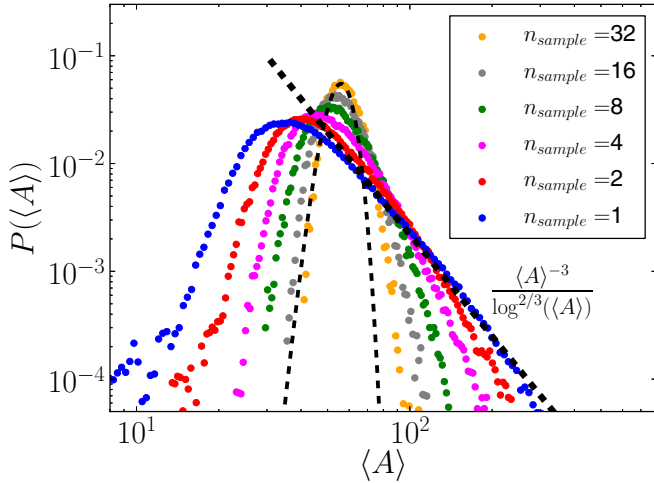


FIG. 10. PDF of sample mean $\langle A \rangle$, over n_{sample} realizations (independent ergophages) from the passive nonlinear point-vortex model with parameters $\delta = 1$, $\nu/\nu_c = 0.15$. For $n_{\text{sample}} = 1$, the PDF is close to the theoretical prediction for the nontruncated system, and converges to a Gaussian PDF (thin dashed line) as n_{sample} is increased.

on the cutoff value ϵ , increasing as the latter is decreased. This is an important difference from the Gaussian noise case. We note, however, that this difference is diminished as larger samples are used due to the imposed truncation and the law of large numbers. This is demonstrated in Fig. 10 which focuses on this power-law tail far from threshold $\nu/\nu_c = 0.15$, and averaging A over independent samples leads to a convergence towards a Gaussian distribution. For a single realization, however, we observe a form close to the theoretical prediction for the nontruncated Lévy process.

C. The fully nonlinear regime

We now enable ergophages to feed back on the point-vortex flow and include the driving velocity \mathbf{u}_f . Initializing a simulation at a condensed vortex state with $\beta = -1/8$, $N_v = 32$ vortices, $N_p = 32$ ergophages at random locations with small initial amplitudes A_k for given values of ν , δ and using a forcing temperature $\beta_f = -1/8$, we let the system evolve in time and measure the mean energy around which the energy fluctuates at late times. The choice $\beta = \beta_f$ for the initial condition is arbitrary, the system will relax to the same stationary state at late times, independently of what initial condition is chosen. However, since we are interested in the stability of condensate flows, it is a natural initial condition.

Figure 11 shows time series of the 2D energy H in the fully nonlinear regime for $\nu/\nu_c = 0.15$ for different values of δ . For large $\delta = 10^6$, the 3D instabilities cannot grow to large amplitudes and therefore do not disrupt the highly energetic condensate. For $\delta = 10^5$, a slightly less energetic condensate persists, but is disrupted at random times by catastrophic events which reduce the 2D flow energy significantly, just to rebuild again thanks to the driving. These are the traces of the jumps associated with Lévy flight dynamics which remain present in the nonlinear regime. Disruptive events occur when an ergophage comes very close to the point-vortex clusters

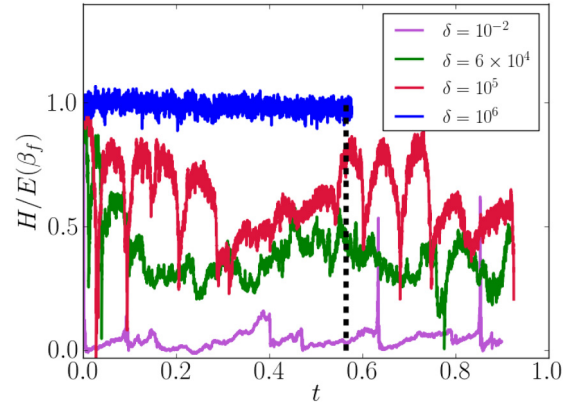


FIG. 11. Time series of the 2D energy H , normalized by the equilibrium energy $E(\beta_f)$ at temperature β_f^{-1} , in the fully nonlinear regime at $\nu/\nu_c = 0.15$ for different values of δ . At $\delta = 10^5$, the flow is close to a 2D condensate, up to abrupt events when the condensate is disrupted. For decreasing values of δ , ergophages grow to larger amplitudes and lower the energy of the 2D flow further. The vertical dashed line indicates the time at which the snapshots in Fig. 12 are taken.

shown in the top panel of Fig. 4, extracting the cluster's energy by partially breaking it up. With decreasing values of δ , the ergophages disrupt the condensate further and further until they reduce its energy to close to zero, driving all point vortices apart. The snapshots of the point-vortex configurations for different δ at a fixed time are shown in Fig. 12. They illustrate the gradual disruption of the condensate as δ is decreased from $\delta = 10^6$ to $\delta = 10^{-2}$.

For each simulation, we use the correspondence between mean energy and inverse temperature visualized in Fig. 2 to assign a vortex temperature based on the measured average point-vortex energy at late times. We repeat this procedure

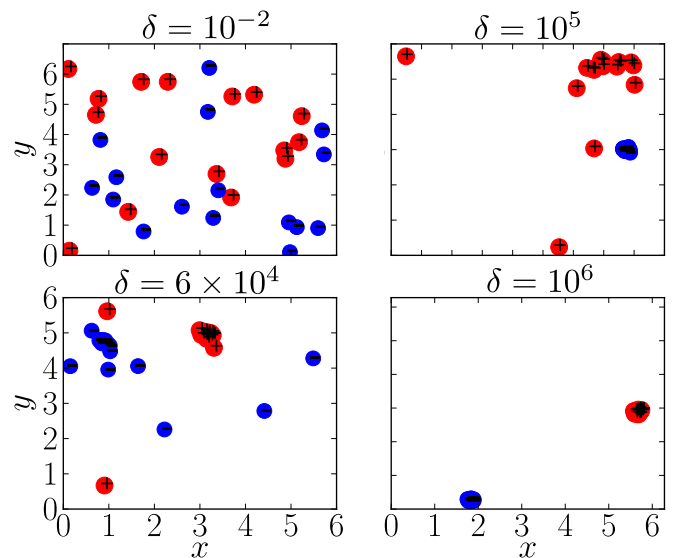


FIG. 12. Snapshots of the point-vortex configuration corresponding to the time indicated by the vertical dashed line in Fig. 11. As δ is decreased, the 3D perturbations are allowed to grow stronger and disrupt the condensate more and more.

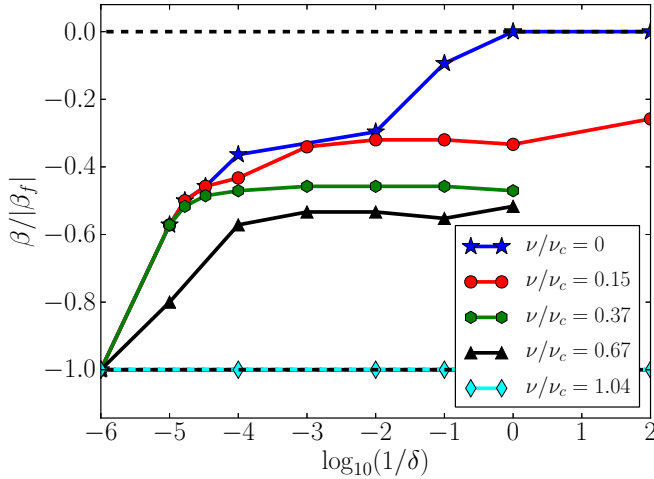


FIG. 13. Plot of mean temperature of the point-vortex flow in a fully nonlinear regime in the presence of $N_p = 32$ perturbations for varying δ , different curves show different ν . At $\nu/\nu_c > 1$, the flow temperature is exactly that of the forcing, i.e., $\beta = \beta_f = -1/8$, since all 3D perturbations decay.

for several values of ν and δ to obtain the diagram shown in Fig. 13.

For $\nu/\nu_c > 1$, 3D perturbations decay and the 2D condensate is stable for all values of δ . As discussed below Eq. (13), where the driving mechanism is defined, the forced system converges to a finite average energy at late times in the absence of ergophages. In other words, the forcing does not inject a constant energy, but acts rather like a thermostat that aims to maintain the system at a fixed temperature. For $\nu/\nu_c < 1$, β increases with decreasing δ . This is the onset three-dimensionality, which we characterized in detail in the passive nonlinear regime. For smaller values of δ , the perturbation amplitudes saturate at larger values, thus disrupting the 2D condensate more strongly. When δ is small enough, the 2D flow reaches $\beta = 0$, which corresponds to a total disruption of the condensate. For $\nu = 0$, this occurs at $\delta = 1$. Since the energy- β curve shown in Fig. 2 is very steep at small energies, small deviations in the energy do not necessarily correspond to vanishing β . Furthermore we note that positive values of β induced by the ergophages were never observed. Since such states would correspond to flows comprised of long-lived bound vortex-antivortex pairs, the absence thereof is consistent with DNS and experiments of turbulent quasi-2D flows, where such configurations do not arise spontaneously.

The role of the remaining parameters β_f , ϵ , N_v , N_p , which do not vary in Fig. 13, is discussed now. Changing β_f would alter the 2D background flow. Decreasing β_f would give a more condensed background flow, reducing the surface area of the vortex clusters and thus the chances that an ergophage comes close enough to a cluster to disrupt it. This would require longer simulations and/or larger N_p to obtain reliable statistics. At larger β_f , the background state ceases to be a condensate, which is undesirable given our focus on condensed base flows. Changing ϵ would affect the minimum inter-vortex distance in the clusters. Decreasing ϵ , the required time step decreases rapidly according to Eq. (15), which is numerically challenging, while larger ϵ would be incompatible

with the strong localization of 3D perturbations. Changing ϵ also affects the mean growth rate and thus ν_c . Finally, we do not expect N_v , N_p to qualitatively change the system behavior. A larger number of vortices making up the condensate implies more 2D energy for ergophages to extract. More ergophages, in turn, are more likely to approach the vortex clusters and thus deplete them. Based on the above discussion, while we did not undertake a systematic parameter study, we expect the qualitative model behavior to be robust to parameter changes within appropriate bounds.

In summary, above the onset of three-dimensionality, studied in detail in the passive nonlinear case, the 2D vortex temperatures depend on the linear and nonlinear damping coefficients of the 3D flow, ranging from a stable condensate to a complete disruption of the latter. The jumplike Lévy flight dynamics discussed for of the linear and weakly nonlinear regimes traces through to the nonlinear regime, and shows in the time series in Fig. 11 by a random disruption of the 2D condensate followed by a rapid subsequent rebuilding of the latter due to the driving.

VI. CONCLUSIONS

We have formulated and analyzed a point-vortex model of localized 3D instabilities on 2D flows. Although the coupling of the 3D perturbations to the 2D flow in the model is ad-hoc and does not stem directly from the Navier-Stokes equations, it has some attractive properties, being energy conserving and reducing to the classical point-vortex model in certain limits. Most importantly, the model has led to some very interesting behaviors and predictions that could apply to more realistic quasi-2D systems exhibiting spectral condensation.

First of all the model predicts fluctuating growth rates with power-law tails, which lead to a Lévy flight in (logarithmic) perturbation amplitude. This may be related to recent DNS results [43], where abrupt, jumplike 3D instabilities were observed on a strongly condensed, turbulent 2D background flow. We point out that in Ref. [43], despite the fact that modern GPU computing power was harnessed and after integrating for long times, the time series in their Fig. 1 only contains a few abrupt growth events, far too few to deduce reliable statistical information about the growth rate. This underscores the need for a simplified model like the one presented here, where such information is more readily accessible. Furthermore the model suggests that the onset of the instability depends on the regularization cutoff ϵ . In realistic flows, a small-scale cutoff is provided by viscosity.

A new type of intermittency near the onset of an instability was discovered. The corresponding situation of on-off intermittency in the presence of ideal, nontruncated Lévy noise, is discussed in the companion paper [72].

In the passive nonlinear regime of the model, we observed a continuous transition from finite to vanishing 3D amplitudes, with on-off intermittent behavior close to onset. However, a deviation from the predictions for Gaussian noise was observed at large values of the 3D amplitude, in the form of a power-law tail whose exponent matches theoretical predictions derived from a fractional Fokker-Planck equation in the companion paper [72]. This exponent also implies that

the saturation amplitude of the second and higher moments would depend on the regularization cutoff ϵ , but not the mean.

In the fully nonlinear, strongly coupled regime, where the vortex temperature is affected by the presence of perturbations, we characterized the dependence of vortex temperature on the ergophage damping coefficients and showed that at large amplitude of the 3D perturbations this temperature reduces to zero. We also showed that at intermediate values of the parameters δ and ν , a highly energetic condensate, present when 3D perturbations are small, is disrupted at random times by catastrophic events where 3D perturbations grow and the condensate amplitude is reduced significantly, after which it recovers. Such events have also been observed in simulations of thin-layer and rotating flows [15,43,74].

In view of the limitations of existing theories, our model provides a new perspective on 3D instabilities growing on 2D flows, which will be useful in analyzing and understanding the much more complex results of DNS and potentially guide further theoretical developments.

ACKNOWLEDGMENTS

We thank three anonymous referees for their comments, which helped us improve the clarity of this paper. We also thank G. Krustolovic for pointing out an important typo in an earlier version of this manuscript. This work was granted access to the HPC resources of MesoPSL financed by the Region Ile de France and the project Equip@Meso (Reference No. ANR-10-EQPX-29-01) of the programme Investissements d'Avenir supervised by the Agence Nationale pour la Recherche and the HPC resources of GENCI-TGCC & GENCI-CINES (Projects No. A0070506421, No. A0080511423, and No. A0090506421), where the present numerical simulations have been performed. This work has also been supported by the Agence nationale de la recherche (ANR DYSTURB Project No. ANR-17-CE30-0004). A.v.K. acknowledges support by Studienstiftung des deutschen Volkes.

APPENDIX A: THE MODEL EQUATIONS FOR PERIODIC BOUNDARY CONDITIONS

In the main text, the model is presented in infinite space for clarity. Here, we describe the case of 2D doubly periodic domain $[0, 2\pi L] \times [0, 2\pi L]$, in which an overall neutral set of an even number N_v of point vortices with circulations $\Gamma_n = (-1)^n \Gamma$, located at positions $\mathbf{x}_v^{(i)} = (x_v^{(i)}, y_v^{(i)})$ move due to their mutual advection. We describe this configuration using the Weiss-McWilliams formalism introduced in Ref. [56]. In addition, as in the main text, we introduce to N_p localized 3D perturbations ("ergophages"), idealized as being pointlike, at positions $\mathbf{x}_p^{(k)} = (x_p^{(k)}, y_p^{(k)})$, which are advected by the 2D point-vortex motions through the 2D domain, and whose amplitude A_k may grow by extracting energy from the 2D flow.

1. Equations of motion and Hamiltonian

The equations of motion of the point vortices and ergophages in the periodic domain are given by the same equations as in the infinite space, Eqs. (2) and (3) along with Eq. (4). The Hamiltonian in the periodic domain differs from

that in the infinite plane, and is given by

$$H(\{\mathbf{x}_v^{(i)} - \mathbf{x}_v^{(j)}\}) = -\frac{1}{2} \sum_{\substack{i,j=1 \\ i \neq j}}^{N_v} \Gamma_i \Gamma_j h(\mathbf{x}_v^{(i)} - \mathbf{x}_v^{(j)}), \quad (\text{A1})$$

with $\mathbf{x}_{vv}^{ij} \equiv \mathbf{x}_v^{(i)} - \mathbf{x}_v^{(j)} \equiv (x_{vv}^{ij}, y_{vv}^{ij})$ and the vortex-pair energy function in the periodic domain given by

$$h(x, y) = \sum_{m=-\infty}^{\infty} \ln \left(\frac{\cosh(x/L - 2\pi m) - \cos(y/L)}{\cosh(2\pi m)} \right) - \frac{x^2}{2\pi L^2}, \quad (\text{A2})$$

where the infinite sum over m stems from the sum over all copies of the periodic domain, as shown in Ref. [56]. A useful alternative notation for the 2D point-vortex advection is given in Ref. [56] as

$$\Gamma_i^{-1} \begin{pmatrix} +\partial_{y_v^{(i)}} H \\ -\partial_{x_v^{(i)}} H \end{pmatrix} = \sum_{\substack{j=1 \\ j \neq i}}^{N_v} \Gamma_j \begin{pmatrix} -S(y_{vv}^{ij}, x_{vv}^{ij}) \\ +S(x_{vv}^{ij}, y_{vv}^{ij}) \end{pmatrix}, \quad (\text{A3})$$

in terms of the rapidly converging series

$$S(x, y) = \frac{1}{L} \sum_{m=-\infty}^{\infty} \frac{\sin(x/L)}{\cosh(y/L - 2\pi m) - \cos(x/L)}. \quad (\text{A4})$$

Equation (A3) relies on the identities $\partial h / \partial x(x, y) = S(x, y) = \partial h / \partial y(y, x)$. We note that at small distances, the periodic copies are negligible and one recovers the results valid in the infinite plane. In particular, for $x, y \ll 1$, $S(x, y) \approx xL / (x^2 + y^2)$. This enables us to transfer all results pertaining to small distances in the infinite plane to the periodic case.

2. Interactions

As in the main text, each of the localized 3D perturbations is assigned an amplitude $A_k \geq 0$, $k = 1, \dots, N_p$, with an associated energy $A_k^2/2$, such that the total energy is again given by Eq. (12), with H given by Eq. (A1). For the velocity $\mathbf{U}_p^{(i)}$ induced by the ergophages on the point vortices, we choose again the form given in Eq. (6). The expression for the dipole field given in Eqs. (7) and (8) must be adapted to satisfy the periodic boundary conditions. This is done by tiling \mathbb{R}^2 with infinitely many copies of the domain $[0, 2\pi L] \times [0, 2\pi L]$ and summing over all copies. For a periodic monopole, one obtains

$$\mathbf{u}_{p,\text{monopole}}^{(k)}(\mathbf{x}) = \nabla \phi^k(\mathbf{x}), \quad (\text{A5})$$

where the potential ϕ^k is given by

$$\phi^k(\mathbf{x}) = h(x - x_p^{(k)}, y - y_p^{(k)}), \quad (\text{A6})$$

in terms of the vortex-pair energy function $h(x, y)$ defined in Eq. (A2). The dipole field arises from the difference between two monopoles at small distances, and it is therefore equal to the derivative of the monopole field along the dipole moment $\hat{d}_k = [\cos(\varphi_k), \sin(\varphi_k)]$,

$$\mathbf{u}_p^{(k)}(\mathbf{x}) = (\hat{d} \cdot \nabla_{\mathbf{x}}) \mathbf{u}_{p,\text{monopole}}^{(k)}(\mathbf{x}). \quad (\text{A7})$$

As in the main text, if the A_k obey Eq. (10) with γ_k given by Eq. (11), then the total energy is conserved in time for arbitrary $\hat{\mathbf{u}}_p$, provided that $\mu = \delta = 0$ (no dissipation), and $\mathbf{u}_f = 0$.

The dipole phase φ_k is an important degree of freedom, which can be adjusted for sustained growth of ergophage amplitude. Indeed, one can rewrite the growth rate as

$$\gamma_k = \Theta_k \cos(\varphi_k) + \Sigma_k \sin(\varphi_k), \quad (\text{A8})$$

with

$$\Theta_k = - \sum_{i=1}^{N_v} \left(\frac{\partial^2 \phi_k(\mathbf{x}_v^{(i)})}{(\partial x_v^{(i)})^2} \frac{\partial H}{\partial x_v^{(i)}} + \frac{\partial^2 \phi_k(\mathbf{x}_v^{(i)})}{\partial x_v^{(i)} \partial y_v^{(i)}} \frac{\partial H}{\partial y_v^{(i)}} \right) \quad (\text{A9})$$

and

$$\Sigma_k = - \sum_{i=1}^{N_v} \left(\frac{\partial^2 \phi_k(\mathbf{x}_v^{(i)})}{\partial x_v^{(i)} \partial y_v^{(i)}} \frac{\partial H}{\partial x_v^{(i)}} + \frac{\partial^2 \phi_k(\mathbf{x}_v^{(i)})}{(\partial y_v^{(i)})^2} \frac{\partial H}{\partial y_v^{(i)}} \right). \quad (\text{A10})$$

The form of Eq. (A8) implies that for any vortex configuration, there is an optimum value of the phases φ_k , for which the growth rate γ_k is at its (positive) maximum, is given by

$$\varphi_k^* = \arctan(|\Sigma_k/\Theta_k|). \quad (\text{A11})$$

The above formulas also apply to dipole ergophages in the infinite domain with the potential Eq. (8). We let $\varphi_k = \varphi_k^*$ for all k at every instant, implying growth of 3D instabilities in the inviscid case.

3. Numerical implementation of the model

We implemented the equations corresponding to Eqs. (2), (3), and (10) with Eqs. (A7) and (A11) in a fully MPI-parallelized Fortran program using a fourth-order Runge-Kutta time stepper. For the numerical implementation, a regularization was introduced at distances smaller than $\epsilon \ll 2\pi L$, for $\epsilon > 0$, in a manner inspired by Ref. [34]. Specifically, we replace

$$h(x, y) \rightarrow \sum_{m=-\infty}^{\infty} \ln \left(\frac{\cosh\left(\frac{x-2\pi mL}{L}\right) - \cos\left(\frac{y}{L}\right) + \epsilon^2}{\cosh(2\pi m)} \right) - \frac{x^2}{2\pi L^2} \quad (\text{A12})$$

and

$$S(x, y) \rightarrow \frac{1}{L} \sum_{m=-\infty}^{\infty} \frac{\sin(x/L)}{\cosh(y/L - 2\pi m) - \cos(y/L) + \epsilon^2}. \quad (\text{A13})$$

As mentioned in the main text, the parallelization is implemented straightforwardly by splitting up the sums over vortex-vortex pairs and vortex-parasite pairs into chunks, each of which is assigned to one processor. The choice of the time step is discussed in the main text.

APPENDIX B: METHOD FOR GENERATING POINT-VORTEX CONFIGURATIONS AT A GIVEN TEMPERATURE

Consider N point vortices located at positions (x_i, y_i) , $i = 1, \dots, N$ in a given finite domain, with associated Hamiltonian H . Pick a positive or negative temperature $T \in \mathbb{R}$. Consider the stochastic gradient dynamics defined by

$$\frac{dx_i}{dt} = -\text{sgn}(T) \frac{\partial H}{\partial x_i} + \sqrt{k_B |T|} \eta_i^{(1)}(t), \quad (\text{B1})$$

$$\frac{dy_i}{dt} = -\text{sgn}(T) \frac{\partial H}{\partial y_i} + \sqrt{k_B |T|} \eta_i^{(2)}(t), \quad (\text{B2})$$

where $\eta_i^{(1)}(t)$ and $\eta_i^{(2)}(t)$ are pairwise independent delta correlated Gaussian noise terms, i.e., $\langle \eta_i^{(1)} \rangle = \langle \eta_i^{(2)} \rangle = 0$ and $\langle \eta_i^{(j)}(t) \eta_{i'}^{(j')}(t') \rangle = 2\delta(t-t')\delta_{i,i'}\delta_{j,j'}$, in terms of the ensemble average $\langle \cdot \rangle$. Denote by \mathbf{X} the state vector with entries $X_{2n-1} = x_n, X_{2n} = y_n$ for $n = 1, \dots, N$. Further, let $\nabla_{\mathbf{X}}$ denote the $2N$ -dimensional gradient operator with respect to \mathbf{X} , then the Fokker-Planck equation for the probability density $P(\mathbf{X}, t)$ associated with the given gradient dynamics reads

$$\partial_t P = \nabla_{\mathbf{X}} \cdot \mathbf{F}, \quad \text{where } \mathbf{F} = \text{sgn}(T)(\nabla_{\mathbf{X}} H)P + k_B |T| \nabla_{\mathbf{X}} P. \quad (\text{B3})$$

In steady state, the flux of probability vanishes if there is no absorption or injection of probability at the boundaries. Solving the zero-flux condition gives the stationary probability density $P_s(\mathbf{X})$,

$$P_s(\mathbf{X}) = \frac{1}{Z} \exp\left(-\frac{H(\mathbf{X})}{k_B T}\right), \quad (\text{B4})$$

which is the Boltzmann equilibrium distribution of the system at temperature T . Thus, solving Eqs. (B1) and (B2) numerically, the system reaches a steady state which is precisely the equilibrium at temperature T . Importantly, adding the Hamiltonian advection term $U_v^{(i)}$ as in Eq. (2) does not change this equilibrium, since the associated terms in the Fokker-Planck equation cancel for every index i (being the divergence of a curl).

APPENDIX C: CONSERVATION OF ENERGY

For the evolution Eqs. (2), (10), and (11), for $\mu = \delta = 0$ and no forcing, one finds that the total energy is conserved, since

$$\frac{dE_{\text{tot}}}{dt} = \frac{dH}{dt} + \sum_{k=1}^{N_p} A_k \frac{dA_k}{dt} \quad (\text{C1})$$

$$= \sum_{i=1}^{N_v} \mathbf{U}_p^{(i)} \cdot \nabla_{\mathbf{x}_v^{(i)}} H + \sum_{k=1}^{N_p} A_k (\gamma_k A_k) \quad (\text{C2})$$

$$= \sum_{i=1}^{N_v} \sum_{k=1}^{N_p} A_k^2 \mathbf{u}_p^{(k)}(\mathbf{x}_v^{(i)}) \cdot \nabla_{\mathbf{x}_v^{(i)}} H - \sum_{k=1}^{N_p} \sum_{i=1}^{N_v} A_k^2 \mathbf{u}_p^{(k)}(\mathbf{x}_v^{(i)}) \cdot \nabla_{\mathbf{x}_v^{(i)}} H \quad (\text{C3})$$

$$= 0. \quad (\text{C4})$$

This conservation of energy is independent of the modeling choice of the velocity field \mathbf{u}_p and of the particular form of the Hamiltonian. Hence the conservation holds for arbitrary boundary conditions.

APPENDIX D: VANISHING MEAN GROWTH RATE FOR MONOPOLE 3D PERTURBATIONS AND DERIVATION OF DIPOLE FORMULAS

The simplest possible choice for the velocity induced by 3D perturbations, $\mathbf{u}_p(\mathbf{x})$, in infinite space is an isotropic radial profile,

$$\mathbf{u}_p^{(k)}(\mathbf{x}) = \frac{\mathbf{x} - \mathbf{x}_p^{(k)}}{|\mathbf{x} - \mathbf{x}_p^{(k)}|^2}, \quad (\text{D1})$$

i.e., a monopole profile. Since it decays at infinity, it is admissible in the infinite plane. In a periodic domain, however, it needs to be adapted to the boundary conditions by summing over an infinite grid of images:

$$\begin{aligned} \mathbf{u}_p(\mathbf{x})^{(k)} &= \sum_{n,m=-\infty}^{\infty} \frac{\mathbf{x} - \mathbf{x}_p^{(k)} - \left(\frac{2\pi n}{2\pi m L}\right)}{|\mathbf{x} - \mathbf{x}_p^{(k)} - \left(\frac{2\pi n}{2\pi m L}\right)|^2} \\ &= \left(\begin{array}{l} S(x - x_p^{(k)}, y - y_p^{(k)}) \\ S(y - y_p^{(k)}, x - x_p^{(k)}) \end{array} \right), \end{aligned} \quad (\text{D2})$$

where $S(x, y)$ is as defined by the rapidly converging series given in Eq. (A4) and regularized in Eq. (A13). Equation (D2) provides an alternative expression for the periodic monopole field, equivalent to that in Eq. (A6). We note that the infinite sum is exactly the double series calculated by Weiss and McWilliams in Ref. [56]. The corresponding growth rate of perturbation k given in Eq. (11) can be rewritten as

$$\gamma_k = \frac{c}{2} \sum_{\substack{i,j=1 \\ i \neq j}}^{N_p} \Gamma_i \Gamma_j \nabla h|_{\mathbf{x}_{ij}^{ij}} \cdot (\nabla h|_{\mathbf{x}_{ij}^{ik}} - \nabla h|_{\mathbf{x}_{ij}^{jk}}), \quad (\text{D3})$$

with $\mathbf{x}_{ij}^{ij} = \mathbf{x}_v^{(i)} - \mathbf{x}_v^{(j)}$ and $\mathbf{x}_{ij}^{ik} = \mathbf{x}_v^{(i)} - \mathbf{x}_p^{(k)}$. It has been used that from Eq. (A4) that $\partial h / \partial x(x, y) = S(x, y) = \partial h / \partial y(y, x)$. For simplicity, since the sum is over vortex pairs, consider a single such pair with circulations Γ_1, Γ_2 at arbitrary positions $\mathbf{x}_1, \mathbf{x}_2$. Place a single ergophage at position (x, y) . The sum over i, j in Eq. (D3) reduces to a single term. Applying the averaging operator over ergophage positions,

$$\bar{F} \equiv \frac{1}{4\pi^2 L^2} \int_0^{2\pi L} \int_0^{2\pi L} F(x, y) dx dy,$$

to the growth rate gives zero, since h is $2\pi L$ -periodic in both the x and y directions. We conclude that the mean growth rate of a monopole ergophage due to a single vortex pair vanishes, for arbitrary vortex positions. Thus, the mean total ergophage growth rate, being the sum of pair contributions, also vanishes. Assuming that for a given vortex configuration, all ergophage positions are equally likely, then the resulting mean growth rate vanishes in the absence of dissipation. When dissipation is added, then 3D perturbations must decay at long times. This is illustrated by a long run with $N_p = 32$ passive nonlinear monopole ergophages and $N_v = 32$ point vortices in Fig. 14.

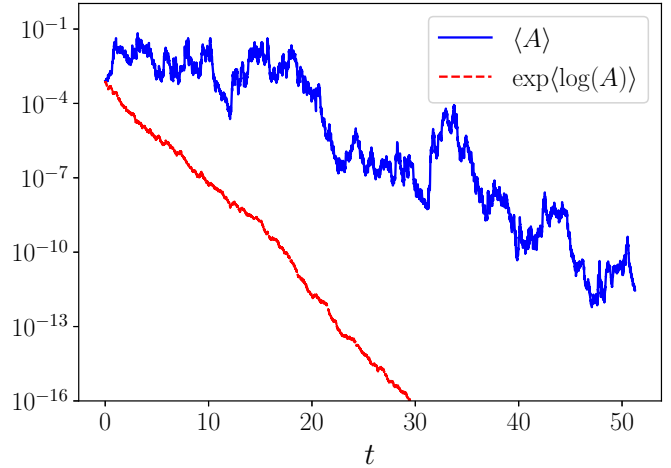


FIG. 14. Lin-log plot of the time series of the first moment $M_1 = \langle A \rangle$ and the zeroth moment $M_0 = \exp(\langle \log(A) \rangle)$ of ergophage amplitude, in terms of the sample average $\langle f(A) \rangle = \frac{1}{N_p} \sum_k f(A_k)$, from a passive nonlinear simulation with $N_p = 32$ ergophages inducing a monopole field, experiencing dissipation $\nu, \delta > 0$. The zeroth moment decays exponentially, indicating that the mean growth rate is negative. Both moments clearly decay at late times as predicted theoretically.

Therefore, the monopole model is insufficient and the dipole model suggests itself as having the minimal complexity to capture mean growth of 3D perturbations.

APPENDIX E: POWER LAWS IN GROWTH RATE PROBABILITY DENSITY

For the dipole parasites introduced in the main text, consider the growth rate of the amplitude of a given ergophage at location \mathbf{x}_p , associated with a vortex pair of circulation Γ_1, Γ_2 at positions $\mathbf{x}_1 = (\ell/2, 0), \mathbf{x}_2 = (-\ell/2, 0)$. We are interested in the tails of the probability density function (PDF), where the ergophage is very close to one or several point vortices, hence boundary conditions are irrelevant and we perform the analysis in the infinite plane. The localized perturbation has a dipole moment $\hat{d} = [\cos(\varphi), \sin(\varphi)]$ attached to it as well as an amplitude A , whose growth rate is given by

$$\begin{aligned} \gamma &= \frac{\Gamma_1 \Gamma_2}{\ell} \left[\frac{\cos(\varphi)}{(x - \frac{\ell}{2})^2 + y^2} \right. \\ &\quad - \frac{2[(\frac{\ell}{2} - x) \cos(\varphi) - y \sin(\varphi)](\frac{\ell}{2} - x)}{[(x - \frac{\ell}{2})^2 + y^2]^2} \\ &\quad - \frac{\cos(\varphi)}{(x + \frac{\ell}{2})^2 + y^2} \\ &\quad \left. + \frac{2[(\frac{\ell}{2} + x) \cos(\varphi) + y \sin(\varphi)](\frac{\ell}{2} + x)}{[(\frac{\ell}{2} + x)^2 + y^2]^2} \right]. \end{aligned} \quad (\text{E1})$$

There are two limits of interest to be considered, namely the *dilute* limit corresponding to small inverse vortex temperatures $|\beta| \ll 1$ and the *dense* limit corresponding to large(-magnitude) inverse vortex temperatures, i.e., pairs of

opposite-sign vortices for $\beta > 0$ and clusters of same-sign vortices for $\beta < 0$.

1. The dilute limit

In this case, the tails of the PDF of γ are generated by events in which the perturbation is closer to a single point vortex than to any other vortices, i.e., $\mathbf{x}_p = \mathbf{x}_1 + r[\cos(\phi), \sin(\phi)]$, $r \ll \ell$. In this case,

$$\begin{aligned} \gamma &\sim \frac{\Gamma_1 \Gamma_2}{\ell r^2} [\sin(\varphi) \sin(2\theta) - \cos(\varphi) \cos(2\theta)] \\ &= -\frac{\Gamma_1 \Gamma_2}{\ell r^2} \cos(2\theta + \varphi). \end{aligned} \quad (\text{E2})$$

Since we consider the case where φ is optimal at every position, one finds $\varphi = -2\theta + n\pi$, $n \in \mathbb{N}$ and

$$\gamma \sim \frac{|\Gamma_1 \Gamma_2|}{\ell r^2} \Leftrightarrow r(\gamma) \sim \sqrt{\frac{\gamma \ell}{|\Gamma_1 \Gamma_2|}}. \quad (\text{E3})$$

Assuming that all ergophage positions are equally probable, then the probability of being at distance between r and $r + dr$ is proportional to the ring area $2\pi r dr$. This can be inverted using Eq. (E3) to obtain a prediction for the PDF of γ , namely,

$$P(\gamma) = r(\gamma) \frac{dr(\gamma)}{d\gamma} \propto \frac{1}{\gamma^2}. \quad (\text{E4})$$

2. The dense limit

In this case, the tails of the PDF of the growth rate stem from encounters of the localized perturbation with pairs of vortices, i.e., $\mathbf{x}_p = r[\cos(\theta), \sin(\theta)]$, $r \gg \ell$. Then, one finds at leading order in ℓ that

$$\begin{aligned} \gamma &\sim \frac{\Gamma_1 \Gamma_2}{\ell} \left(-2\ell \frac{\cos(\varphi) \cos(\theta)}{r^3} \right. \\ &\quad \left. + 2\ell \frac{y \sin(\varphi)(y^2 - 3x^2) - 2x \cos(\varphi)(x^2 - y^2)}{r^6} \right) \\ &\sim -\frac{2\Gamma_1 \Gamma_2}{r^3} \cos(3\theta - \varphi) \end{aligned}$$

Again assuming that φ is optimal, then $\varphi = -3\theta + n\pi$, $n \in \mathbb{N}$, such that

$$\gamma \sim \frac{2|\Gamma_1 \Gamma_2|}{r^3},$$

which leads to the growth rate PDF, again under the assumption that all ergophage positions are equally probable,

$$P(\gamma) = r(\gamma) \frac{dr(\gamma)}{d\gamma} \propto \frac{1}{\gamma^{\frac{1}{3} + \frac{4}{3}}} = \frac{1}{\gamma^{5/3}},$$

with an exponent $-5/3$, whose magnitude is less than 2. For both cases (dense and dilute), the PDF has neither a finite mean, nor a finite variance. We note that the exponent $-5/3$ found here bears no relation to Kolmogorov's spectral exponent, it is merely a consequence of the modeling choices made.

-
- [1] H. v. Helmholtz, LXIII. On integrals of the hydrodynamical equations, which express vortex-motion, *London, Edinburgh, Dublin Philos. Mag. J. Sci.* **33**, 485 (1867).
- [2] G. Kirchhoff, *Vorlesungen Über Mathematische Physik: Mechanik* (B. G. Teubner, Leipzig, 1876), Vol. 1.
- [3] P. G. Saffman and D. Meiron, Difficulties with three-dimensional weak solutions for inviscid incompressible flow, *Phys. Fluids* **29**, 2373 (1986).
- [4] C. Greengard and E. Thomann, Singular vortex systems and weak solutions of the Euler equations, *Phys. Fluids* **31**, 2810 (1988).
- [5] J. Goodman, T. Y. Hou, and J. Lowengrub, Convergence of the point vortex method for the 2D Euler equations, *Commun. Pure Appl. Math.* **43**, 415 (1990).
- [6] L. Onsager, Statistical hydrodynamics, *II Nuovo Cimento* (1943–1954) **6**, 279 (1949).
- [7] G. L. Eyink and K. R. Sreenivasan, Onsager and the theory of hydrodynamic turbulence, *Rev. Mod. Phys.* **78**, 87 (2006).
- [8] R. H. Kraichnan and D. Montgomery, Two-dimensional turbulence, *Rep. Prog. Phys.* **43**, 547 (1980).
- [9] P. Tabeling, Two-dimensional turbulence: A physicist approach, *Phys. Rep.* **362**, 1 (2002).
- [10] G. Boffetta and R. E. Ecke, Two-dimensional turbulence, *Annu. Rev. Fluid Mech.* **44**, 427 (2012).
- [11] U. Frisch and A. N. Kolmogorov, *Turbulence: The Legacy of A.N. Kolmogorov* (Cambridge University Press, Cambridge, UK, 1995).
- [12] A. Celani, S. Musacchio, and D. Vincenzi, Turbulence in More Than Two and Less than Three Dimensions, *Phys. Rev. Lett.* **104**, 184506 (2010).
- [13] H. Xia, D. Byrne, G. Falkovich, and M. Shats, Upscale energy transfer in thick turbulent fluid layers, *Nat. Phys.* **7**, 321 (2011).
- [14] S. J. Benavides and A. Alexakis, Critical transitions in thin layer turbulence, *J. Fluid Mech.* **822**, 364 (2017).
- [15] A. van Kan and A. Alexakis, Condensates in thin-layer turbulence, *J. Fluid Mech.* **864**, 490 (2019).
- [16] S. Musacchio and G. Boffetta, Condensate in quasi-two-dimensional turbulence, *Phys. Rev. Fluids* **4**, 022602(R) (2019).
- [17] L. M. Smith, J. R. Chasnov, and F. Waleffe, Crossover from Two-to Three-Dimensional Turbulence, *Phys. Rev. Lett.* **77**, 2467 (1996).
- [18] E. Deusebio, G. Boffetta, E. Lindborg, and S. Musacchio, Dimensional transition in rotating turbulence, *Phys. Rev. E* **90**, 023005 (2014).
- [19] A. Alexakis and L. Biferale, Cascades and transitions in turbulent flows, *Phys. Rep.* **767**, 1 (2018).
- [20] E. D. Siggia and H. Aref, Point-vortex simulation of the inverse energy cascade in two-dimensional turbulence, *Phys. Fluids* **24**, 171 (1981).
- [21] G. F. Carnevale, J. C. McWilliams, Y. Pomeau, J. B. Weiss, and W. R. Young, Evolution of Vortex Statistics in Two-Dimensional Turbulence, *Phys. Rev. Lett.* **66**, 2735 (1991).

- [22] R. Benzi, M. Colella, M. Briscolini, and P. Santangelo, A simple point vortex model for two dimensional decaying turbulence, *Phys. Fluids A* **4**, 1036 (1992).
- [23] J. B. Weiss and J. C. McWilliams, Temporal scaling behavior of decaying two-dimensional turbulence, *Phys. Fluids A* **5**, 608 (1993).
- [24] E. Trizac, A coalescence model for freely decaying two-dimensional turbulence, *Europhys. Lett.* **43**, 671 (1998).
- [25] J. B. Weiss, Punctuated hamiltonian models of structured turbulence, in *Semi-Analytic Methods for the Navier–Stokes Equations*, edited by K. Coughlin, *CRM Proc. Lecture Notes* **20**, 109 (1999).
- [26] H. Aref, Stirring by chaotic advection, *J. Fluid Mech.* **143**, 1 (1984).
- [27] M. P. Rast and J.-F. Pinton, Point-vortex model for lagrangian intermittency in turbulence, *Phys. Rev. E* **79**, 046314 (2009).
- [28] M. P. Rast and J.-F. Pinton, Pair Dispersion in Turbulence: The Subdominant Role of Scaling, *Phys. Rev. Lett.* **107**, 214501 (2011).
- [29] M. P. Rast, J.-F. Pinton, and P. D. Mininni, Turbulent transport with intermittency: Expectation of a scalar concentration, *Phys. Rev. E* **93**, 043120 (2016).
- [30] B. Gallet and R. Ferrari, The vortex gas scaling regime of baroclinic turbulence, *Proc. Natl. Acad. Sci. USA* **117**, 4491 (2020).
- [31] L. Horace, *Hydrodynamics*, 6th ed. (Dover, New York, 1945).
- [32] H. Aref and E. D. Siggia, Evolution and breakdown of a vortex street in two dimensions, *J. Fluid Mech.* **109**, 435 (1981).
- [33] R. Krasny, A study of singularity formation in a vortex sheet by the point-vortex approximation, *J. Fluid Mech.* **167**, 65 (1986).
- [34] R. Krasny, Desingularization of periodic vortex sheet roll-up, *J. Comput. Phys.* **65**, 292 (1986).
- [35] B. Nowak, J. Schole, D. Sixty, and T. Gasenzer, Nonthermal fixed points, vortex statistics, and superfluid turbulence in an ultracold bose gas, *Phys. Rev. A* **85**, 043627 (2012).
- [36] M. T. Reeves, T. P. Billam, B. P. Anderson, and A. S. Bradley, Inverse Energy Cascade in Forced Two-Dimensional Quantum Turbulence, *Phys. Rev. Lett.* **110**, 104501 (2013).
- [37] T. P. Billam, M. T. Reeves, B. P. Anderson, and A. S. Bradley, Onsager-Kraichnan Condensation in Decaying Two-Dimensional Quantum Turbulence, *Phys. Rev. Lett.* **112**, 145301 (2014).
- [38] A. Griffin, V. Shukla, M.-E. Brachet, and S. Nazarenko, Magnus-force model for active particles trapped on superfluid vortices, *Phys. Rev. A* **101**, 053601 (2020).
- [39] G. Joyce and D. Montgomery, Negative temperature states for the two-dimensional guiding-centre plasma, *J. Plasma Phys.* **10**, 107 (1973).
- [40] P.-H. Chavanis, J. Sommeria, and R. Robert, Statistical mechanics of two-dimensional vortices and collisionless stellar systems, *Astrophys. J.* **471**, 385 (1996).
- [41] B. Gallet, Exact two-dimensionalization of rapidly rotating large-Reynolds-number flows, *J. Fluid Mech.* **783**, 412 (2015).
- [42] B. Gallet and C. R. Doering, Exact two-dimensionalization of low-magnetic-Reynolds-number flows subject to a strong magnetic field, *J. Fluid Mech.* **773**, 154 (2015).
- [43] K. Seshasayanan and B. Gallet, Onset of three-dimensionality in rapidly rotating turbulent flows, *J. Fluid Mech.* **901**, R5 (2020).
- [44] E. M. Purcell and R. V. Pound, A nuclear spin system at negative temperature, *Phys. Rev.* **81**, 279 (1951).
- [45] A. Oja and O. Lounasmaa, Nuclear magnetic ordering in simple metals at positive and negative nanokelvin temperatures, *Rev. Mod. Phys.* **69**, 1 (1997).
- [46] P. Medley, D. M. Weld, H. Miyake, D. E. Pritchard, and W. Ketterle, Spin Gradient Demagnetization Cooling of Ultracold Atoms, *Phys. Rev. Lett.* **106**, 195301 (2011).
- [47] Y. Yatsuyanagi, Y. Kiwamoto, H. Tomita, M. M. Sano, T. Yoshida, and T. Ebisuzaki, Dynamics of Two-Sign Point Vortices in Positive and Negative Temperature States, *Phys. Rev. Lett.* **94**, 054502 (2005).
- [48] X. Yu, T. P. Billam, J. Nian, M. T. Reeves, and A. S. Bradley, Theory of the vortex-clustering transition in a confined two-dimensional quantum fluid, *Phys. Rev. A* **94**, 023602 (2016).
- [49] F. Cornu and B. Jancovici, On the two-dimensional coulomb gas, *J. Stat. Phys.* **49**, 33 (1987).
- [50] G. Krstulovic, C. Cartes, M. Brachet, and E. Tirapegui, Generation and characterization of absolute equilibrium of compressible flows, *Int. J. Bifurcat. Chaos* **19**, 3445 (2009).
- [51] L. Biferale, Shell models of energy cascade in turbulence, *Annu. Rev. Fluid Mech.* **35**, 441 (2003).
- [52] M. D. Bustamante and S. Nazarenko, Derivation of the Biot-Savart equation from the nonlinear Schrödinger equation, *Phys. Rev. E* **92**, 053019 (2015).
- [53] R. Hänninen and A. W. Baggaley, Vortex filament method as a tool for computational visualization of quantum turbulence, *Proc. Natl. Acad. Sci. USA* **111**, 4667 (2014).
- [54] J. C. McWilliams, The emergence of isolated, coherent vortices in turbulent flow, in *AIP Conference Proceedings* (American Institute of Physics, College Park, MD, 1984), Vol. 106, pp. 205–221.
- [55] H. Kellay, Hydrodynamics experiments with soap films and soap bubbles: A short review of recent experiments, *Phys. Fluids* **29**, 111113 (2017).
- [56] J. B. Weiss and J. C. McWilliams, Nonergodicity of point vortices, *Phys. Fluids A* **3**, 835 (1991).
- [57] R. Courant, K. Friedrichs, and H. Lewy, Über die partiellen differenzgleichungen der mathematischen physik, *Math. Ann.* **100**, 32 (1928).
- [58] D. J. Acheson, *Elementary Fluid Dynamics*, Oxford Applied Mathematics and Computing Science Series (Oxford University Press, Oxford, UK, 1990).
- [59] A. A. Dubkov, B. Spagnolo, and V. V. Uchaikin, Lévy flight superdiffusion: An introduction, *Int. J. Bifurcat. Chaos* **18**, 2649 (2008).
- [60] B. B. Mandelbrot, *The Fractal Geometry of Nature* (W. H. Freeman, New York, 1983), Vol. 173.
- [61] M. F. Shlesinger, G. M. Zaslavsky, and U. Frisch, *Lévy Flights and Related Topics in Physics* (Springer, Berlin, 1995).
- [62] R. Klages, G. Radons, and I. M. Sokolov (eds.), *Anomalous Transport: Foundations and Applications* (John Wiley & Sons, 2008).
- [63] I. Min, I. Mezić, and A. Leonard, Levy stable distributions for velocity and velocity difference in systems of vortex elements, *Phys. Fluids* **8**, 1169 (1996).

- [64] W. Horsthemke, Noise induced transitions, in *Non-equilibrium Dynamics in Chemical Systems* (Springer, Berlin, 1984), pp. 150–160.
- [65] N. Platt, E. A. Spiegel, and C. Tresser, On-Off Intermittency: A Mechanism for Bursting, *Phys. Rev. Lett.* **70**, 279 (1993).
- [66] S. Aumaître, K. Mallick, and F. Pétrélis, Noise-induced bifurcations, multiscaling and on–off intermittency, *J. Stat. Mech.: Theory Exp.* (2007) P07016.
- [67] S. J. Benavides, E. A. Deal, M. Rushlow, J. G. Venditti, Q. Zhang, K. Kamrin, and J. T. Perron, The impact of intermittency on bed load sediment transport (2021), <https://doi.org/10.31223/X5PW3Q>.
- [68] M. Ding and W. Yang, Distribution of the first return time in fractional Brownian motion and its application to the study of on-off intermittency, *Phys. Rev. E* **52**, 207 (1995).
- [69] A. Alexakis and F. Pétrélis, Planar bifurcation subject to multiplicative noise: Role of symmetry, *Phys. Rev. E* **80**, 041134 (2009).
- [70] A. Alexakis and F. Pétrélis, Critical exponents in zero dimensions, *J. Stat. Phys.* **149**, 738 (2012).
- [71] F. Pétrélis and A. Alexakis, Anomalous Exponents at the Onset of an Instability, *Phys. Rev. Lett.* **108**, 014501 (2012).
- [72] A. van Kan, A. Alexakis, and M.-E. Brachet, Lévy on-off intermittency, *Phys. Rev. E* **103**, 052115 (2021).
- [73] R. N. Mantegna and H. E. Stanley, Stochastic Process with Ultraslow Convergence to a Gaussian: The Truncated Lévy Flight, *Phys. Rev. Lett.* **73**, 2946 (1994).
- [74] A. van Kan, T. Nemoto, and A. Alexakis, Rare transitions to thin-layer turbulent condensates, *J. Fluid Mech.* **878**, 356 (2019).